Journal of Techniques, ISSN: 2708-8383, Vol. 7, No. 4, 2025, Pages 53-67
DOI: https://doi.org/10.51173/jt.v7i4.2776

JOURNAL OF TECHNIQUES

Journal homepage: http://journal.mtu.edu.iq

RESEARCH ARTICLE – MECHANICAL ENGINEERING

Resistance Spot Welding of Dissimilar Metals (AISI 1005 and AISI 304L): Experimental and Numerical Investigation of Tensile-Shear and Vibration Loads

Osamah Sabah Barrak[1, 2*], Hadhami Ben Slama[1], Slim Ben-Elechi[1], Sami Chatti[1]

[1]National Engineering School of Monastir, University of Monastir, LGM, ENIM, Avenue Ibn-Eljazzar, 5019 Monastir, Tunisia

[2]Polytechnic College of Engineering – Baghdad, Middle Technical University, Baghdad, Iraq

[*] Corresponding author E-mail: usamah.barrak@mtu.edu.iq

Article Info.

Article history:

Received
10 November 2025

Revised
10 December 2025

Accepted
20 December 2025

Published
31 December 2025

Abstract

This study investigates the resistance spot welding (RSW) of two different steels, AISI 1005 and AISI 304L, using both experiments and computer simulations. Researchers used a Taguchi L16 design to test how welding current, squeeze time, welding time, and hold time affect tensile-shear strength (TSF). The best welding setup reached a TSF of 78.86 MPa, while the lowest settings gave 44.31 MPa. Simulations in COMSOL Multiphysics modeled the thermal, electrical, and mechanical behavior of the welds. The predicted TSF values matched the experiments closely, with less than 5% difference. Free-vibration modal analysis was also done for cantilever and fixed-fixed setups. The experimental and simulated eigenfrequencies were similar, with errors within ±3%, supporting the accuracy of the model. These results show that choosing the right RSW parameters can greatly improve both the strength and stiffness of AISI 1005/AISI 304L joints.

Publisher: Middle Technical University

Keywords: Vibration Analysis; Eigenfrequency; Finite Element Analysis (FEA); Resistance Spot Welding (RSW); Sustainable Manufacturing.

1. Introduction

Welding is the joining of metal by heat, with or without added pressure and/or filler metal [1, 2]. Thousands of spot welds are typically used in automotive manufacturing, providing excellent dynamic and structural characteristics to the vehicle [3, 4]. A fusion welding process that uses melting to join metallic parts is called spot welding. Resistance Spot Welding (RSW) is a popular option for auto-body assembly, truck cabins, rail cars, and home appliances because of its distinct advantages, which include low cost, high speed, and automation applicability [5-7]. The resistance spot welding (RSW) method is typically used in electronic, automotive, and aerospace components to join thin metal plates [8-11]. More than a thousand RSW joints can be observed in a vehicle, and most of them must be able to support external weights [12-14]. The RSW process is less expensive, more efficient, has a smaller heat-affected zone, less deformation and stress, and is easier to operate, as compared with other welding techniques [15–18]. Welding parameters are optimised to improve the resistance spot welding (RSW) process, promoting green manufacturing with energy and material savings and enabling lighter, eco-efficient structures in automotive and aerospace applications. As a result, some automotive engineering parts are made using dissimilar-metal RSW. The strength of RSW joints is heavily influenced by welding parameters, e.g., current time and clamping forces. Improper welding conditions can cause incomplete penetration, burn-through, splashing, fractures, cracks, and porosity [19–21].

It is difficult to join dissimilar materials because the procedure requires that the materials' mechanical, chemical, and physical characteristics match [22, 23]. As automobiles are developing quickly, using different steels for several engineering components is necessary to reduce weight, cost, and material consumption. These different steels are often combined using the RSW technique to ensure sufficient joining strength. However, because the two types of steels have different chemical compositions and mechanical qualities, employing the RSW method on dissimilar steels is complicated. Additionally, the welding conditions significantly impact the RSW joints of dissimilar steels [10, 24, 25]. The appropriate welding parameters must be determined to establish a strong connection between mild carbon steel (St.) and stainless steel (St. St.) [26, 27]. Due to the benefits of the weld joint, joining different materials has recently acquired increasing popularity in industries [28]. In addition to becoming commonly utilised for various applications requiring a specific combination of properties, the primary purpose of material combination is to provide a more optimal, lightweight, and high-performance structure to gain the necessary product performance and save cost [29, 30].

Nomenclature & Symbols

RSW	Resistance Spot Welding	FEA	Finite Element Analysis
IMC	Intermetallic Components	EMA	Experimental Modal Analysis
FE	Finite Element	St.	Mild Carbon Steel
St. St.	Stainless Steel	TSF	Tensile-Shearing Force
Wc	Welding Current	wt	Welding Time
sq.t.	Squeeze Time	ht	Hold Time
SIER	State Company for Inspection and Engineering Rehabilitation	DOE	Design of Experiments
3D	Three Dimensional	Q	Heat Generated (Joules)
I	Welding Current (Amperes)	R	Electrical Resistance at the Welding Spot (Ohms)
t	Time of Current Flow (Seconds)	ρ	Density (kg/m^3)
c_p	Specific Heat Capacity (J/kg K)	T	Temperature (K)
k	Thermal Conductivity (W/m K)	Q_{gen}	Heat Generation Rate Per Unit Volume (W/m^3)
R(T)	Resistance at temperature T (Ohms)	R_0	Resistance at Reference Temperature T_0 (Ohms)
α	Temperature Coefficient of Resistance (1/K)	m	Mass (kg)
K	Stiffness (N/m)	x	Displacement (m)
HAZ	Heat Affected Zone	w_n	Angular Natural Frequency
f_n	Natural Frequency (Hertz)	OP	Optimal Sample

Furthermore, compared to RSW joints constructed from similar metals, the quality of RSW joints formed of dissimilar metals is more susceptible to the welding current (wc), welding time (wt), and electrode force. These factors have made it extremely difficult for the automotive industry to combine plates of different metals [31, 32].

In recent years, some research has focused on RSW joints of dissimilar metals under different experimental conditions. Li et al. [33] presented a hybrid resistance laser spot welding technique. Steel and 6016-T4 aluminum alloy were welded using the RSW technique; then, a laser spot welding process was used to further join the steel and aluminum alloy. The findings indicated that the welding joints made using this technique had tensile-shear forces 18.2% higher than those of a single RSW operation. Aslanlar et al. [34, 35] studied the influences of welding parameters on the tensile strength of RSW joints of steel alloy plates. It was found that 11 kA for 10 times and 10 kA for 12 and 15 periods induced the highest tensile strength. Kianersi et al. [36] investigated the effects of welding parameters on the microstructure and mechanical characteristics of AISI 316 L austenitic stainless-steel sheets. The tensile-shear strength of RSW joints rose with increasing welding current, while strength was reduced due to the nugget size expansion. The failure mode changed from exclusively interfacial to entirely tearing around the nugget as the welding current increased. Wu et al. [37] used the RSW technique on galvanized steel sheets with different welding parameters. They discovered that raising heat input increased the shear strength of RSW joints. Nevertheless, the expulsion problem could reduce shear strength when the welding current and welding time are increased further. It is possible to overlook the effects of welding time and welding current on the stiffness of RSW joints. Mohsen et al. [38] analysed the shear strength of the dissimilar metals (stainless steel and aluminum alloy) combined by the RSW technique. It was discovered that using a welding current of 11.86 kA can enhance the shear strength and extend the diameter of the RSW joints, and the nugget's grain size was reduced. However, a notable number of intermediate phases were found at the steel-aluminum contact, which weakened the RSW joints' shear strength. Zhang et al. [39] analysed the microstructure and mechanical characteristics of austenitic stainless-steel alloy and 6063-T6 aluminum alloy RSW joints under various welding conditions. Their results showed that increasing the welding current and time can increase the nugget's diameter. A double-layer complex of phases was produced at the aluminum/steel interface, and increasing the intermetallic components (IMC) layer increased the strength of the RSW joints within a specific range. The nugget's diameter approximated 5.4 mm, the RSW joint's tensile strength was 1.783 kN, the welding time was 200 ms, the electrode pressure was 2 kN, the welding current was 7 kA, and the fracture mechanism was interfacial. Mansor et al. [40] used the RSW process to weld the dissimilar austenitic stainless steel 316 L and titanium alloy by employing various varieties of welding conditions. The tensile-shear strength of RSW joints was more significantly affected by the welding current (51.68%), after welding time (20.41%) and electrode force (27.91%).

Modal analysis is the technique of determining an elastic structure's modes of vibration to describe its dynamic properties. Each mode has a unique natural frequency and damping factor that can be determined from almost any point on the structure. This accurate prediction of structural dynamic characteristics (e.g., natural frequency and damping ratio) is significant for vibration suppression and performance assurance under dynamic conditions [41, 42]. Modal testing using an impact hammer is a test method that allows researchers to measure natural frequencies (modes), damping, and mode shapes, which are the focus of EMA techniques. Since the force used when hammering cannot be maintained during the experiment, the impact hammer test is a simple procedure but challenging to get reliable findings. Additionally, using impulse, this method can provide quicker measurement durations with minimal equipment requirements. The finite element (FE) approach is the most widely used numerical technique for simulating the behavior of natural systems. Analysis, prediction, and design are the three primary components that comprise the objective of numerical modeling [43-45]. FE analysis simulation is a computerized approach to the investigation of structures.

Finite Element Model (FEM) updating is a process to reduce the disparities between analytical and experimental outcomes. It seems that it is complicated to chuck the errors and inaccuracies in FEM when the structure under consideration is complex. Numerous approaches to updating structural models have been presented, and the case is still involved in research in several fields. Most of these works focused on approaches like maximum matrix updating [46] and sensitivity-based parameter assessment [47]. Many researchers are currently studying a variety of alternative model updating procedures, including the perturbation method [48], stochastic [49], and Bayesian model updating [22]. Several investigators in model updating have developed, applied, researched, and commented on these strategies [50-52].

Previous studies on resistance spot welding (RSW) have broadly investigated similar and dissimilar materials without giving sufficient attention to specific alloy combinations. In the present study, RSW is applied to low-carbon steel AISI 1005 and stainless steel AISI 304L to address this gap and provide deeper insights into the welding behavior of dissimilar steels. The tensile-shear strength of the welded joints was systematically evaluated under variable welding conditions, including welding current, squeeze time (sq.t.), welding time, hold time (ht), and constant electrode force. To complement the experiments, a finite element model was developed in COMSOL Multiphysics to simulate both tensile-shear and vibration responses.

Comparisons with experimental and numerical results showed the reliability of the prediction model, with deviations mainly well within acceptable bounds. In contrast to previous works that have largely focused on static performance or microscopic characterizations, the present study couples macroscopic and dynamic analyses with a high-fidelity numerical simulation, enabling a systematic understanding of the correlations between process conditions and joint performance. The verified model also demonstrates a promising role in assisting in the optimization of parameter settings towards improved joint integrity and cost-effectiveness for automotive and aerospace applications.

2. Experimental Procedures

St. AISI 1005 and St. St. AISI 304L were joined employing the RSW technique. Table 1 exhibits the experimental weight for the chemical compositions of the metals analysed at the Engineering Institute. and the lab. Department, State Company for Inspection and Engineering Rehabilitation (SIER), Ministry of Industry and Minerals, Baghdad, Iraq, while Table 2 indicates the material properties of the metals. The specimens used in this study have dimensions that meet the requirements of the AWS C1.1M/C1.1:2012 standard [53].

Table 1. Chemical composition of AISI 304L and AISI 1005

Element wt.%	C%	Si%	Ni%	P%	S%	Cr%	Mo%	Mn%	V%	Cu%	Fe%
AISI 304L	0.027	0.52	11.24	0.032	0.005	18.89	0.002	1.53	0.008	0.246	Bal.
AISI 1005	0.08	-	0.024	0.01	0.026	0.04	-	0.38	-	0.048	Bal.

Table 2. Material properties of AISI 304L and AISI 1005

Material Property	AISI 304L	AISI 1005
Yield Strength (MPa)	305	184
Tensile Strength (MPa)	610	325
Elongation El. (%)	62	33
Young's modulus (GPa)	193	200
Density (kg/m^3)	8000	7850
Poisson's ratio	0.28	0.29
Thermal conductivity (W/(m·K))	16.2	52
Coefficient of thermal expansion (K)	17.2x10^{-6}	12x10^{-6}
Heat capacity at constant pressure (J/(kg·K))	500	450
Electrical conductivity (S/m)	1.4 x10^6	6.99x10^6
Relative permittivity	10^6	10^6

Fig. 1 displays the measurements of sheet metal AISI 304L and AISI 1005, which are 25 x 100 mm with an overlap width of 25 x 25 mm and a thickness of 1 mm. The metal surfaces were initially meticulously cleaned with acetone using an ultrasonic cleaner for five minutes. The RSW method uses a procedure with a specific kind of conical electrode. The electrodes (type E Truncated) were composed of a chromium-zirconium-copper alloy with good electrical and thermal conductivity and had a 20-truncated conical form with a 5 mm circular contacting surface [38].

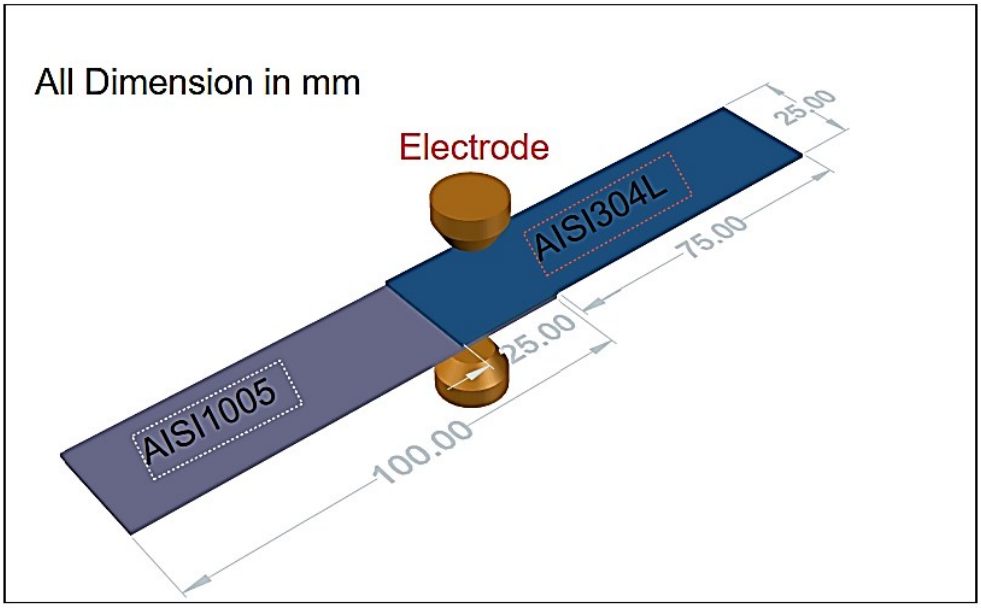

Fig. 1. A schematic diagram of the specimen

With a constant electrode pressure of 0.2 MPa, the specimens were prepared for the RSW method with a range of welding conditions, including wc from 4 kA to 7 kA, sq.t. from 0.6 to 1.2 s, wt from 0.8 to 1.4 s, and ht from 0.8 to 1.4 s. To study the influences of welding parameters on the tensile-shearing force (TSF) of RSW joints, the Design of Experiments (DOE) made an orthogonal examination (Taguchi method) matrix with four components and four levels. A Taguchi L16 (4^4) orthogonal array was used to study four factors, each at four levels. Each welding sample was tested three times (n = 3), and the order was randomized to reduce bias. Range analysis was used to identify the factor that most affects the TSF of RSW process joints. Fig. 2 displays the welding parameters. A tensile test machine examined the sample RSW joint's TSF.

The rate of deformation was kept constant at 1 mm/min. To avoid a bending moment during the tensile shear test, sample spacers of 1 mm in thickness were attached to the test specimens' edges.

Performed free-vibration tests using classical experimental modal analysis (EMA) to verify the numerical eigenfrequency results for both cantilever and fixed-fixed support setups. The welded specimens were mounted on a rigid steel fixture that matched the boundary conditions used in the finite element model. For the cantilever setup, one end was clamped while the other remained free. For the fixed-fixed setup, both ends were clamped. During testing, a single, short force pulse was applied at each excitation point, and the free-decay response was measured. Identified eigenfrequencies and mode shapes from the measured Frequency Response Functions (FRFs) using peak-picking and curve-fitting methods, following standard EMA procedures.

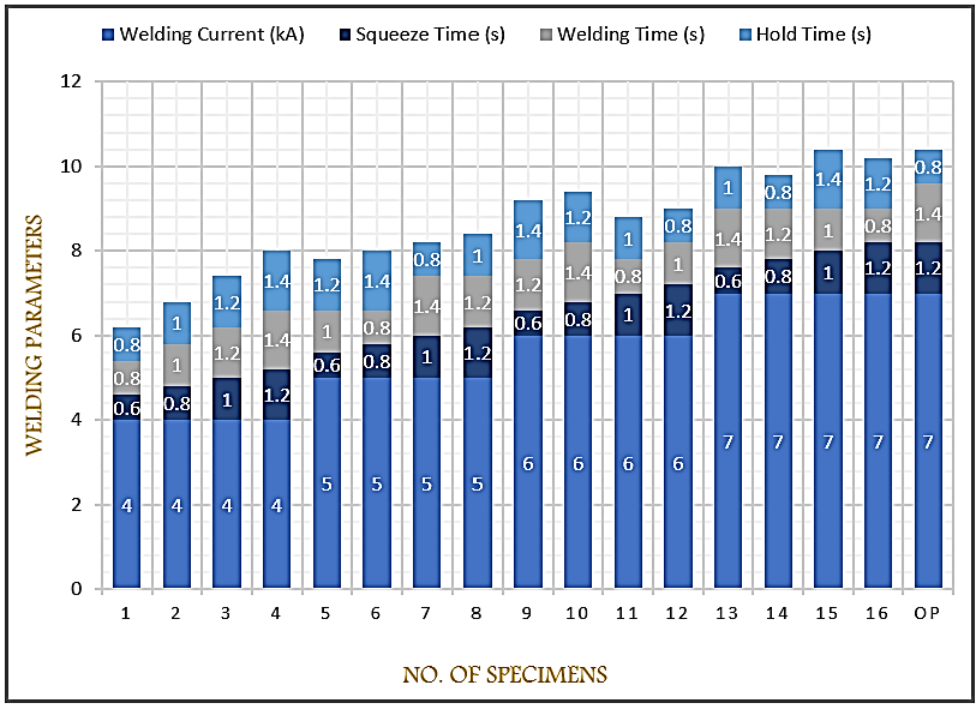

Fig. 2. Welding parameters

In this research, the tensile-shearing test of RSW joints was performed to achieve an accurate estimation outcome. The TSF of the different dissimilar plates is shown in Fig. 3.

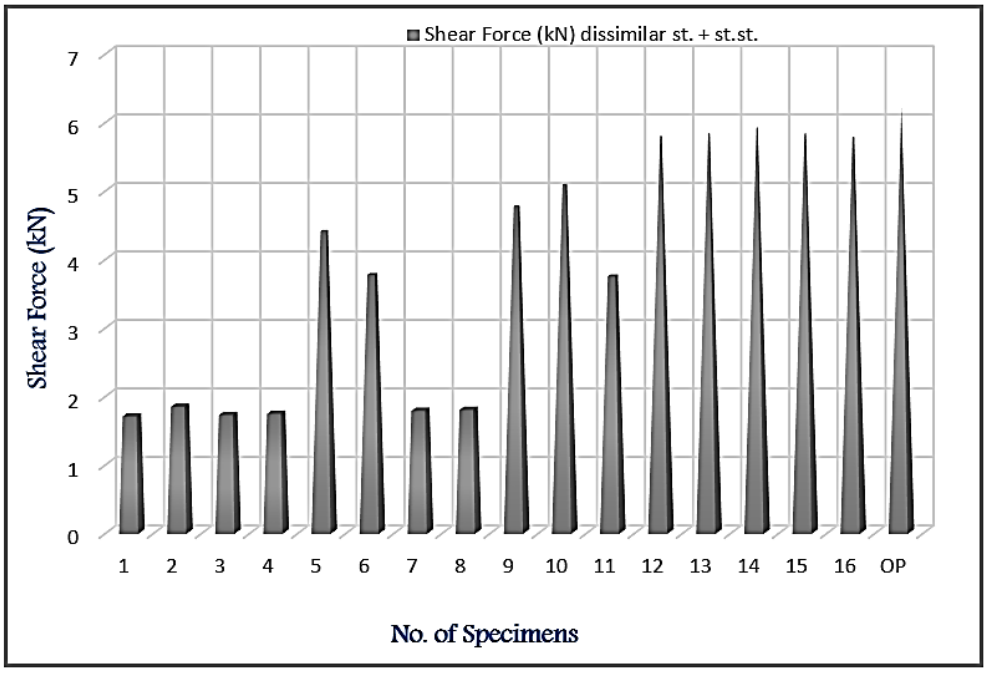

Fig. 3. Tensile shear force

3. Finite Element Analysis

In this research, spot weld joints were numerically analysed utilising the COMSOL Multiphysics commercial finite elements tool. Metal joints that were single spot-welded using lap shear were considered. It is essential to utilise a detailed, precise spot-weld finite element model for dynamic structural analysis, which presents a good analysis for static stress and dynamic analysis because a spot-welded joint affects the vibrational properties of engineering structures. 3D shell elements with reduced integration order were used to represent the metal sheet of the spot-welded joint (Fig. 4). Then, the tensile shear test, the natural frequencies, and mode shapes were extracted from COMSOL Multiphysics.

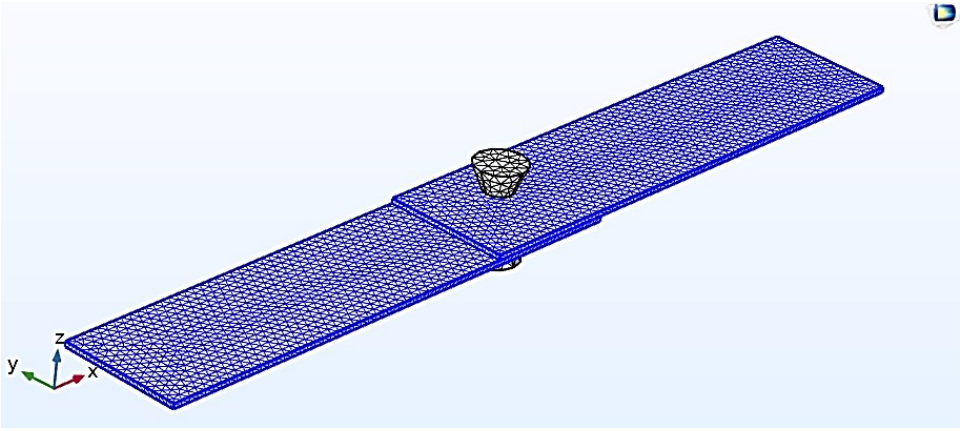

Fig. 4. 3D mesh elements

4. Simulation Model

The RSW method uses a procedure with a specific kind of conical electrode. This research conducted three simulation models: the first model of the RSW joint, the second model for the tensile-shear test of the RSW joint, and the third model for the vibration test of the RSW joint. Three physics were used to produce the model of the RSW joint, known as the multi-physics model, which includes electric currents, heat transfer in solids, and solid mechanics. Simulation Model was conducted on the samples of the RSW joint No.1, No.6, No.OP that achieved minimal, middle, and maximum values of TSF, respectively, employing the eq. 1-3 [15]. Material properties required for simulation models are shown in Table 2. The tensile-shear test model of the RSW joint was conducted using solid mechanics physics.

4.1. Equations for RSW

The heat generated as a result of Electrical Resistance [54, 55]:

$$Q = I^2 R t \quad (1)$$

Q: Heat generated (Joules), I: Welding current (Amperes), R: Electrical resistance at the welding spot (Ohms), and t: Time of current flow (Seconds). Transient Heat Conduction Equation (Heat Equation) [56]:

$$\rho c_p \frac{\partial t}{\partial T} = \nabla \cdot (k \nabla T) + Qgen \quad (2)$$

ρ: Density (kg/m³), c_p: Specific heat capacity (J/kg K), T: Temperature (K), t: Time (Seconds), k: Thermal conductivity (W/m K), and Q_{gen}: Heat generation rate per unit volume (W/m³). Temperature Dependence of Electrical Resistance [57]:

$$R(T)=R_0 [1+\alpha(T-T_0)] \quad (3)$$

R(T): Resistance at temperature T (Ohms), R_0: Resistance at reference temperature T_0 (Ohms), α: Temperature coefficient of resistance (1/K), and T, T_0: Temperature (K).

4.1. Equations for vibration test

The vibration test model of the RSW joint was performed by employing solid mechanics physics, which is dependent on random vibration and can be analytically evaluated as a first degree of freedom-free vibration with cantilever and fixed-fixed support. The analytical solution to the eigenvalue trouble for a first degree of freedom-free vibration with cantilever and fixed-fixed support can be discovered in [58, 59]. It can be computed employing the eq. 4-8 [60, 61]:

- Motion for Undamped Free Vibration Equation:

$$m\frac{d^2x}{dt^2} + Kx = 0 \quad (4)$$

m: Mass (kg), K: Stiffness (N/m), and x: Displacement (m).

- Angular Natural Frequency:

$$w_n = \sqrt{\frac{k}{m}} \quad (5)$$

- Natural Frequency (Hertz):

$$f_n = \frac{w_n}{2\pi} \tag{6}$$

- First Natural Frequency for a Cantilever:

$$f_1 = \frac{1.875^2}{2\pi L^2}\sqrt{\frac{EI}{\rho A}} \tag{7}$$

- First Natural Frequency for a Fixed-Fixed:

$$f_1 = \frac{4.73^2}{2\pi L^2}\sqrt{\frac{EI}{\rho A}} \tag{8}$$

E: Young's modulus (GPa), I: Moment of inertia (cross-section) (m^4), A: Cross-sectional area (m^2), and L: Length of the beam (m).

5. Results and Discussion

5.1. FEA simulation of RSW

A simulation of the RSW process was performed for the three samples (OP, No.6, No.1) to study the effect of different welding conditions on the material properties. Fig. 5 indicates the simulation results of the RSW process, which studies the effect of the process on the distribution of von Mises stresses for the specimens. The results show the stress distribution during and after the RSW method for the samples (OP, No.6, No.1).

The OP sample indicates that the von Mises stresses at the end of the welding simulation process mainly focus on the center of the spot welding. The high-stress values of 0.89 MPa demonstrate the formation of a high-stress zone that undergoes mechanical changes throughout the cooling phase. The higher stress values for samples No. 6 and No. 1 were 0.65 MPa and 0.45 MPa, respectively, which imply outdated stresses. It exhibits weaker stress diffusion, even though there are fewer mechanical and thermal consequences during welding.

The exerted cooling and the material properties of the welding type are seen to have a considerable effect on the stress distribution, as shown by simulation results. The heat-affected zone (HAZ) may contain high levels of residual stresses, which may adversely affect the mechanical behaviour, as evidenced by the stress–strain diagram of the OP sample [62, 63]. To improve the specimen's structural performance, samples No.6 and No.1 exhibited more stable conduct with less stress effect, confirming the feasibility of particular techniques to regulate stress distribution during and after the RSW process. This result ascertains the conclusions of Johnson and Miller [64], who noted the advantages of welding parameter optimisation to optimise post-welding stress distribution and lessen the thermal effect.

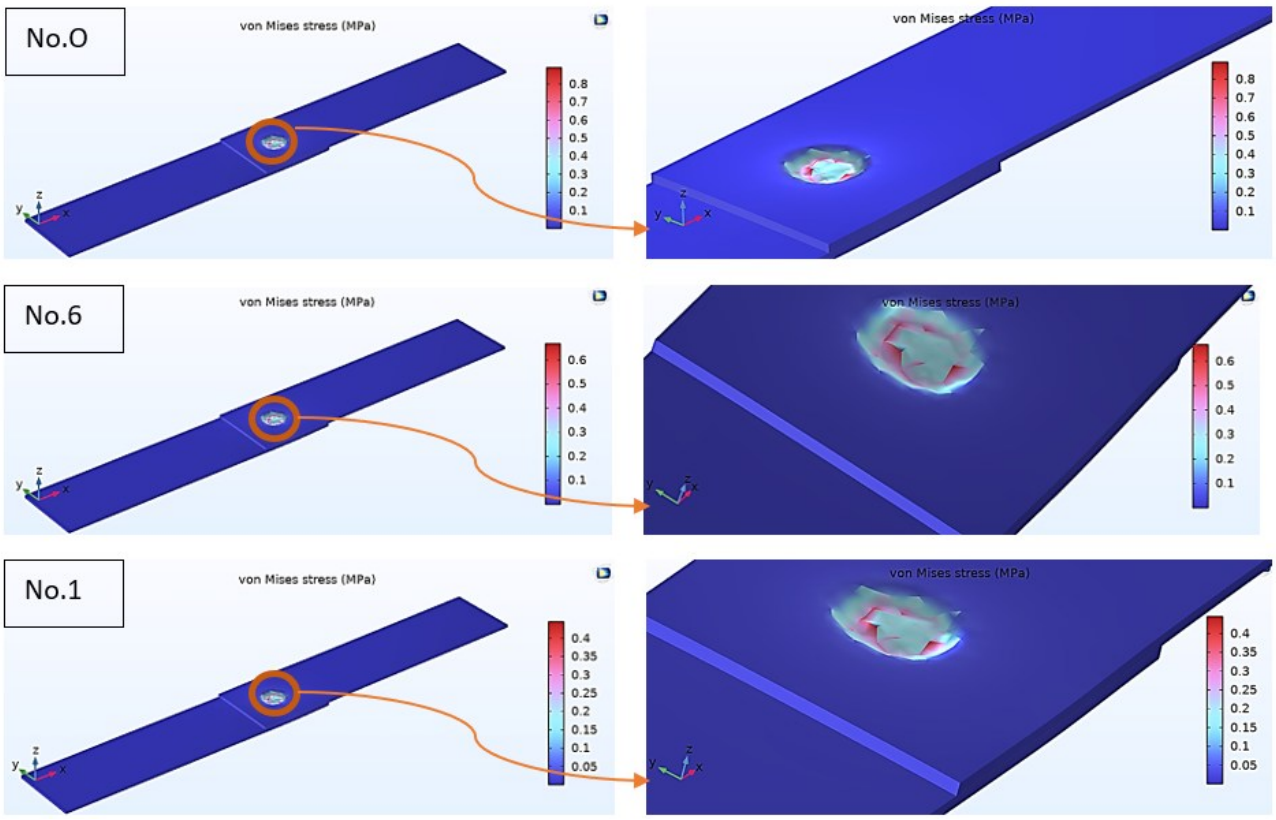

Fig. 5. Simulation of welding (Von Mises Stress)

Fig. 6 displays a simulation of the equivalent deviatoric strain of samples (OP, No.6, and No.1) during and after the RSW process, providing an understanding of the deformation attributes and potential weak points in the RSW joint. The simulation of the specimen OP shows that strain in the weld zone reaches high levels during RSW, with magnitudes up to about 38×10^{-7}. This suggests that the OP weld parameters may lead to increased strain accumulation during welding, resulting in considerable local deformation. The equivalent deviatoric strain in the OP specimen decreases during the RSW process, but it has consistently attracted significant attention at the spot weld. This internal stress may affect the dynamic endurance of the weld. The more typical strain distribution of the Specimen No.6 has a maximum strain of approximately 30×10^{-7}. The decrease in strain intensity indicates that the welding condition of No.6 resulted in more well-regulated deformation, which is beneficial to the stability inhibition of the weld joint during RSW one. This strain after RSW shows a more homogeneous distribution and a lower peak strain than the specimen OP. It indicates that the Mid. C composition tends to promote a more stable weld with less residual stress/current. Under welding, the specimen No.1 attains the minimum equivalent deviatoric strain, and the peak strain is almost 20×10^{-7}. It shows the RSW conditions for No. 1, resulting in the best strain distribution and limiting extensive deformation during RSW. Compared after welding, sample No. 1 would still have the lowest strain concentration and a better strain release process, with a higher probability of maintaining weld quality during service life. It may achieve better performance under vibration loading. The results indicated that proper welding conditions should be adopted to reduce strain distribution in RSW joints and improve mechanical properties [65, 66].

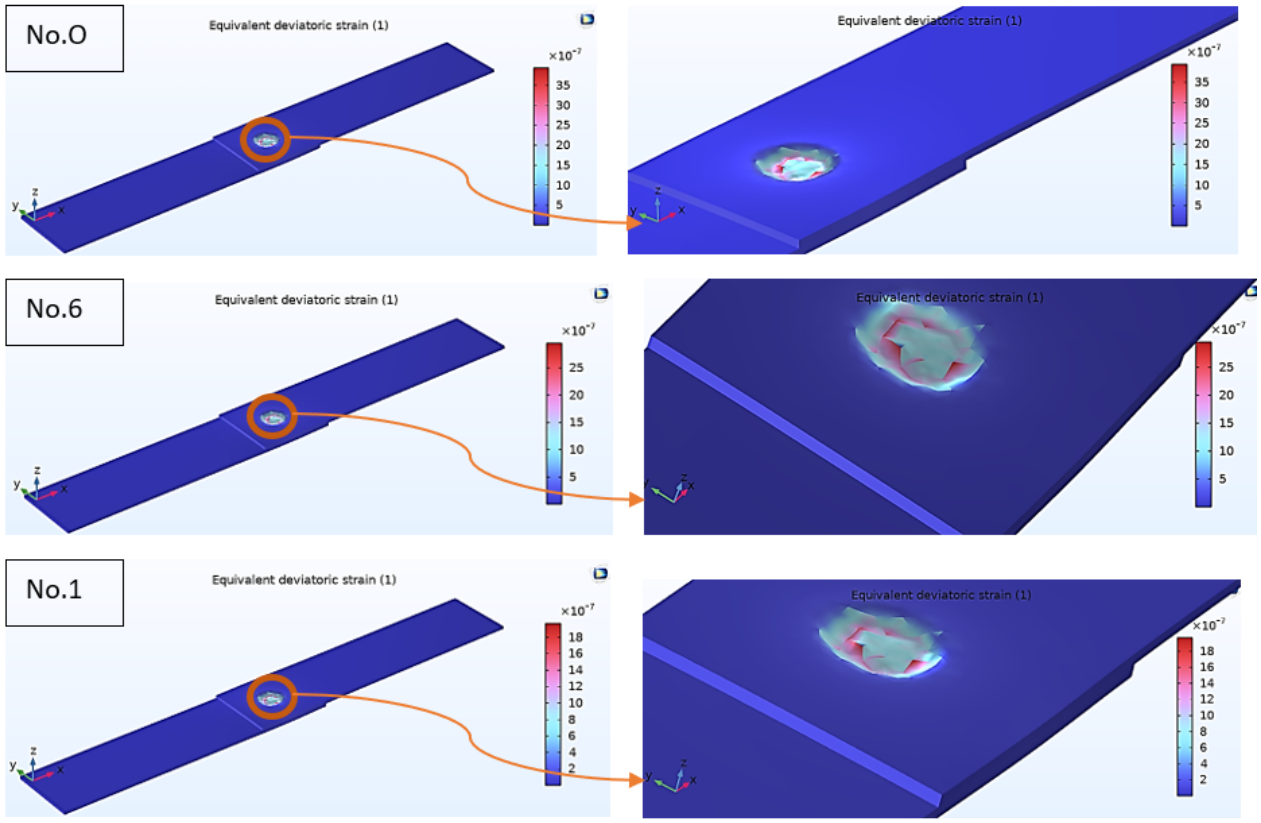

Fig. 6. Simulation of welding (Equivalent Deviatoric Strain)

5.2. Tensile-shear strength simulation of RSW

The tensile test results for the samples (OP, No.6, and No.1) indicate the distribution of von Mises stress (MPa), as shown in Fig. 7. These studies show the stress distribution and deformation parameters of each specimen's mechanical behavior under tensile loading. In the sample OP, the von Mises stress is distributed particularly in the welded area, with the highest stress values being around 500 MPa. The high concentration is present in the weld nugget and the HAZ, which shows that the OP welding conditions may have caused significant residual stresses in these regions. The specimen's OP elevated stress level can have resulted from hardening or brittleness close to the weld zone, which might have been produced by excessive heat input from the welding current or insufficient cooling from the short hold time. Because these stress concentrations can operate as locations for crack initiation under the tensile load, they are disturbing because they may cause premature failure. The stress exhibits a fast drop-off from the spot region toward the base metal, indicating inadequate stress distribution and a sudden change in material characteristics between the spot region and base metal; Fig. 8 shows the sample OP after the tensile test. This sudden change may further increase the possibility of the weld failure under strain. In contrast to the specimen OP, the specimen No.6 exhibits a relatively more uniform distribution, indicating improved stress in the welded zone, even if its von Mises stress is more moderate, with peak stress values approaching 350 MPa. The No.6 welding parameters probably included optimal heat input from welding current and cooling rates from hold time to balance the spot weld zone and HAZ, as indicated by the decrease in peak stress values. This modification reduces the chance of crack initiation under applied tensile load and does not allow for residual stress. The triangle specimen (No. The relatively uniform stress distribution in the spot weld zone suggests that the welding methods and so on for the specimen (No. 1) were appropriate for mitigating residual stresses. The stress distributions in the HAZ and weld zone indicate that the mechanical properties are consistent. Such stability could result from tight regulation of parameters such as current, welding time, and squeezing time, thereby reducing the stress that accumulates during weld formation. The simulation results highlight the importance of welding parameters on the mechanical behaviour of weld connections under tensile loading

conditions. Sample OP shows that hardening or stress zones may be caused by poor welding methods, leading to a high gradient and a high concentration of stress. These weak spots, which could lead to a poor weld, may compromise the weld's structural integrity, leaving it vulnerable to early failure. This was consistent with prior research reporting that when the welding duration and current are low, higher residual stress (Park et al., 2020; Zhao and Wang, 2018) [67, 68] and poor mechanical performance are observed. The samples OP and No. 1, on the other hand, demonstrated superior stress distribution patterns and lower peak stresses. Hence, the welding conditions used are a factor in reducing the likelihood of fracture under tensile stress, most notably in the OP structure. Because they help balance the mechanical properties in the spot weld zone and HAZ. Sequential adjustment of welding current, squeeze time, and hold time during RSW can significantly improve joint quality by reducing residual stresses and improving stress distribution, as reported in the literature (Chen and Lee, 2019; Huang et al., 2021). [69, 70]. In the specimen OP, the transitional stress spreading from the fusion zone to the base metal region results in a high-strength joint with reduced fracture risk. These data further highlight the importance of using ideal welding conditions for structural integrity, particularly under high-tensile loads. Especially, the specimen OP will be most useful when durability and load-bearing are required in many applications, due to its homogeneous stress distribution.

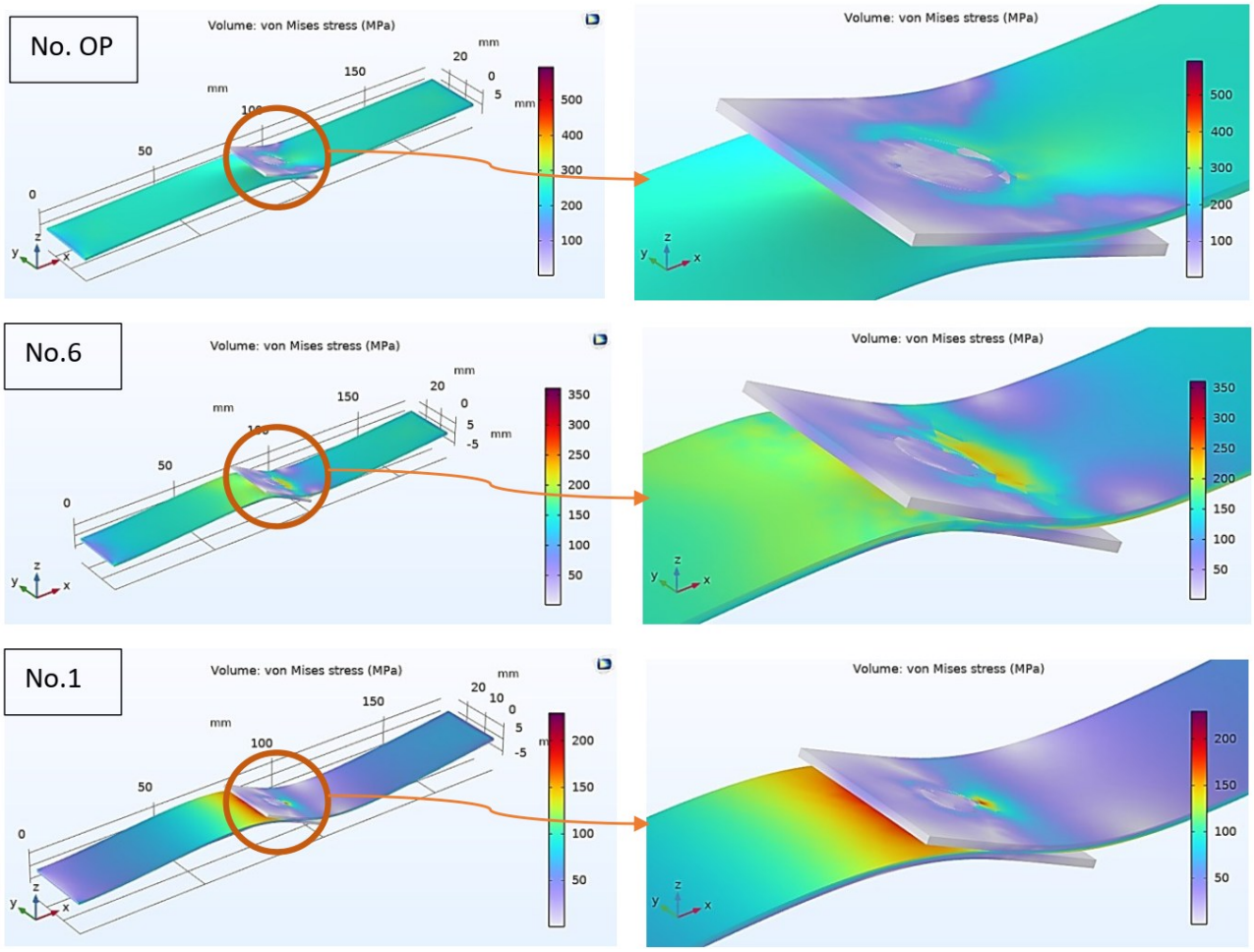

Fig. 7. Simulation of tensile test

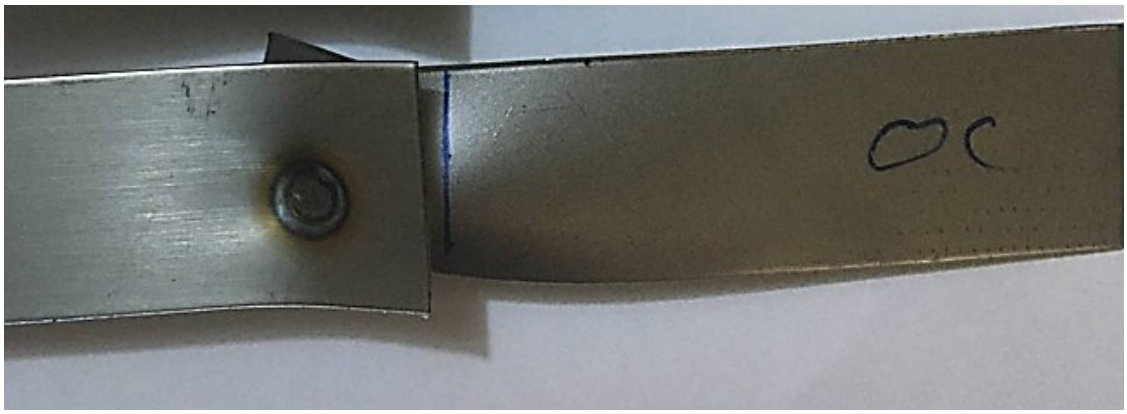

Fig. 8. Sample No.OP after the tensile test

5.3. Tensile-shear test validation

Table 3 compares the simulation and experimental shear stress values (OP, No.6, and No.1) for each sample and provides an error percentage estimate for each. This is necessary for validating the reliability of the simulation model used to predict the behavior of welded joints. A deviation of 4.3% arises from the OP of the OP for 75.45 MPa compared to the experimental result at 78.86 MPa for the specimen (OP value left as simulated). So, this correlation between the calculated and simulated data suggests that the simulation model properly describes the mechanical behavior of the specimen under tensile-shear loading, and it confirms that the RSW parameter model is valid, as a very low error value near zero was observed. The simulation results can be considered credible for further investigation of the OP behavior of the specimen under various loading conditions. The comparisons between the simulated and experimental values for samples No. 6 and No. 1 reveal improvement rates of 4.56% and 4.8%, respectively. The higher error with respect to the OP sample could indicate that deviations in the RSW parameters within weld jointing can lead to discrepancies in the ability of simulation models to correctly predict performance in experiments for this configuration. The simulation results are reliable, though the error has increased slightly. Modeling inaccuracies are caused by the thermal and mechanical influences of each welding condition on the difference. Prior research has demonstrated that RSW welding parameters (welding current, welding time, and squeeze time) can lead to changes in mechanical properties that affect shear strength [71, 72]. Thus, the simulation results' accuracy could be enhanced to some extent by correcting the model and RSW parameters.

Table 3. Tensile-shear stress validation

No. of Specimens	Simulation value (MPa)	Experimental value (MPa)	Error
OP	75.45	78.86	4.3%
No.6	56.45	59.15	4.56%
No.1	42.18	44.31	4.8%

5.4. Vibration test simulation

Eigenfrequency results from vibration test simulations provide key data on the dynamic behaviour of the welded specimens (OP, No.6, and No.1) under different support conditions, such as cantilever and fixed-fixed. The eigenfrequencies are the natural frequencies at which the 2-DOF system vibrates, and they depend largely on boundary conditions, material parameters, and structural stiffness. The cantilever support has a fixed end and a free end, resulting in decreased overall stiffness and, consequently, lower eigenfrequencies. It is also shown in Tables 4 and 5 that all the specimens have almost the same eigenfrequencies: No. 1 (25.859 Hz), No.6. (25.894 Hz), and OP (25.846). In other words, the first vibration mode is primarily governed by the system's mass and the overall geometry relevant to the weld parameters. In particular, there are some significant differences in modes (2–5). The eigenfrequency of the OP is highest (870.02 Hz) for Mode 5, e.g., than No.6 (868.22 Hz) and No.1 (852.82 Hz). The decreased stiffness for No.1 is characterised by a softer structure, which results in good stress rehabilitation and a uniform spot-welding zone. The eigenfrequencies at the cantilever fixed end are typically larger in higher modes for sample OP, and an analysis suggests this is due to the stiffer local vicinity around spot welds, as well as the local residual stress introduced by optimal welds. The higher mode eigenfrequencies of sample No. 1 indicate enhanced internal stresses and more effective energy dissipation, leading to greater stiffness and flexibility in response to dynamic loading.

Compared with the cantilever support, the fixed-fixed support has higher frequencies at both ends and is significantly higher than the former, because it has a higher structural stiffness under these boundary conditions (Tables 6 and 7). For mode 1 with OP (147.25 Hz), No. 6 (148.23 Hz), and No.l (147.15 Hz), the eigenfrequencies are larger for the fixed-fixed support than for the visc. Fixed-fixed cantilever type of supporting structure, as well as a new type of improved trapezoidal four-strip curtain pivotal structure. It is observed from this comparison that, while it is still faster in frequency, the thrust purely space-target fundamental mode identified below results in only 28. The stiffest response among the modes, No. 6, is observed for this mode in the present configuration. As shown, large discrepancies are observed at the second through fifth modes: both OP (1530.4 Hz) and No.6 (1530.1 Hz) have the largest eigenfrequencies at Mode 5, only slightly larger than that of No.1 (1526 Hz). In higher modes, sample No. 1 generally shows lower eigenfrequencies, indicating a better distribution of strain energy and damping. The fixed-fixed support resulted in higher structural stiffness than the cantilever support, causing a shift of all eigenfrequencies to higher values across all samples. OP exhibits the highest eigenfrequencies in higher modes, which imply stiffer weld properties stemming from asymmetric stress distribution on account of higher residual stress. The reduced eigenfrequencies of Min. C. exhibit an evenly distributed stress profile and high-quality welding, thereby reducing rigidity and enhancing vibration absorption.

On the one hand, there are freezing conditions at the two ends of the free surfaces, while on the other hand, it is fixed and far from the bimaterial interface. The eigenfrequency and the absolute value of the Von Mises stress are computed by the finite element method using COMSOL. The result shows excellent consistency with that reported in this paper. Due to its free-end flexibility, the cantilever configuration has lower eigenfrequencies and allows higher deformation under vibration. The sample OP shows that the eigenfrequencies remain relatively high throughout both support conditions, especially at higher modes. Such effects, due to residual stresses and localized stiffness in the spot weld area, may impact long-term durability and fatigue strength; this underscores the importance of optimal welding conditions to enhance the dynamic performance of welded joints.

Table 4. First degree of freedom-free vibration with cantilever (Eigenfrequency (Hz))

Mode	OP	No.6	No.1
1	25.846	25.894	25.859
2	152.26	152.6	152.77
3	351.59	350.24	347.01
4	458.2	458.21	457.29
5	870.02	868.22	852.82

Table 5. First degree of freedom-free vibration with cantilever beam (Von Mises Stress)

Mode	OP	No.6	No.1
1	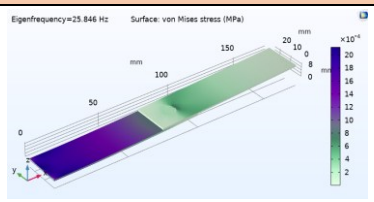	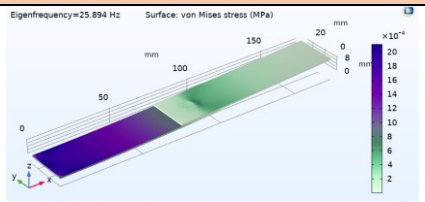	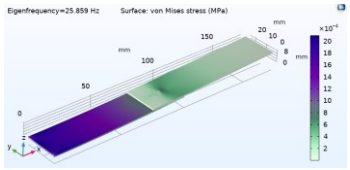
2	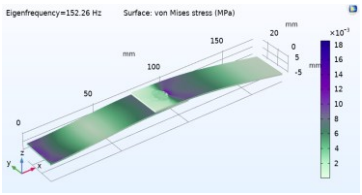	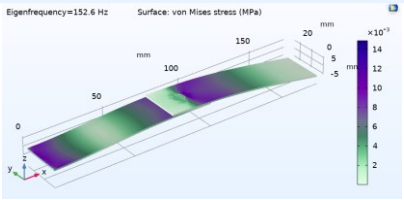	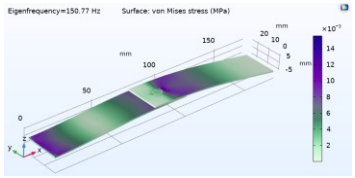
3	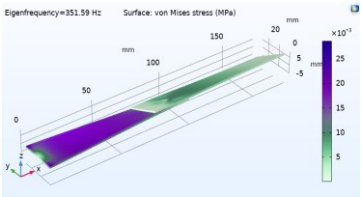	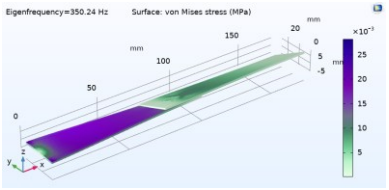	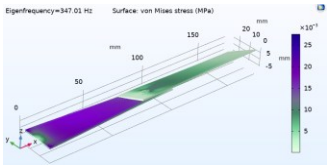
4	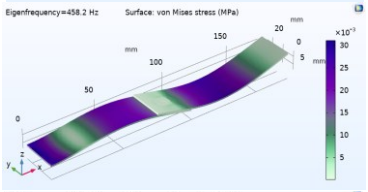	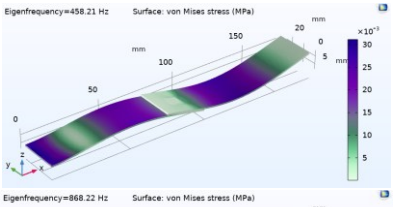	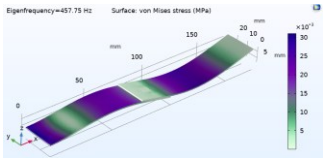
5	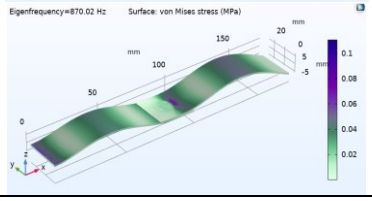	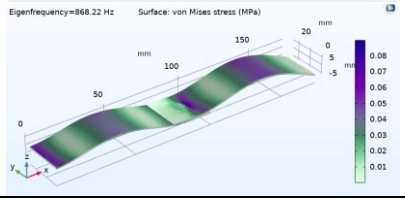	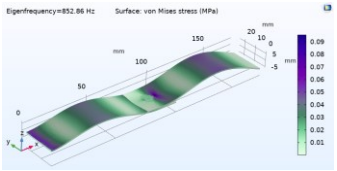

Table 6. First degree of freedom-free vibration with fixed-fixed support (Eigenfrequency (Hz))

Mode	OP	No.6	No.1
1	147.25	148.23	147.15
2	531.56	530.89	529.08
3	670.07	671.22	670.09
4	876.77	876.773	859.14
5	1530.4	1530.1	1526

Table 7. First degree of freedom-free vibration with fixed-fixed support (Von Mises Stress)

Mode	OP	No.6	No.1
1	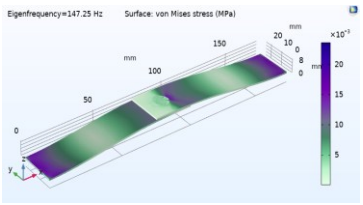	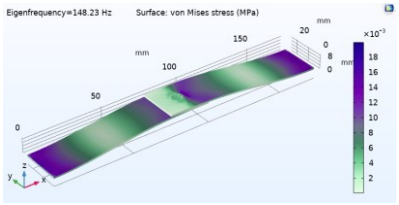	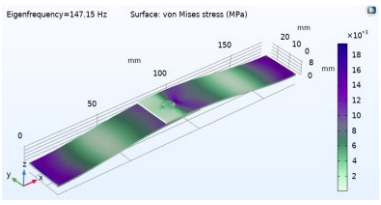
2	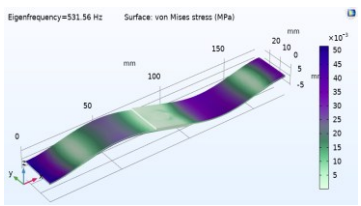	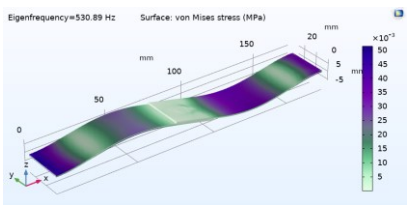	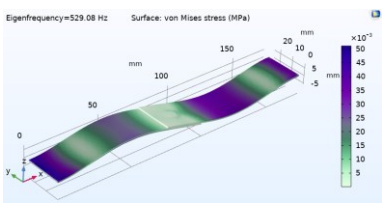

Continue Table 7. First degree of freedom-free vibration with fixed-fixed support (Von Mises Stress)

3	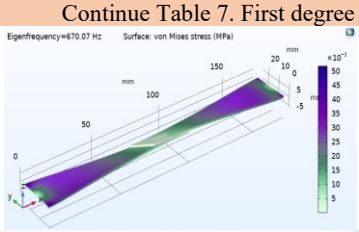	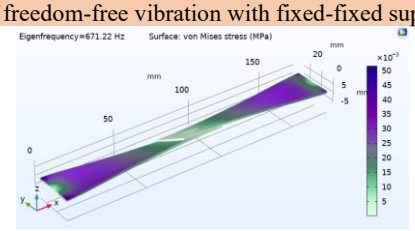	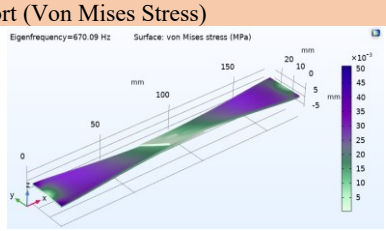
4	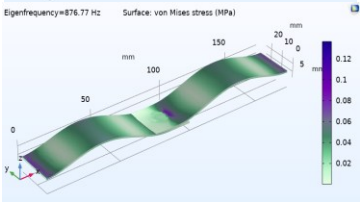	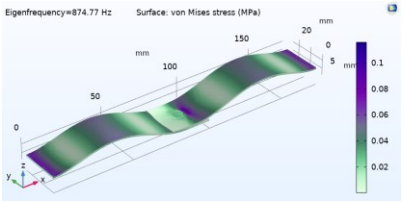	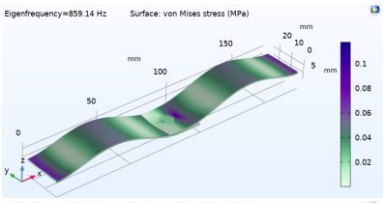
5	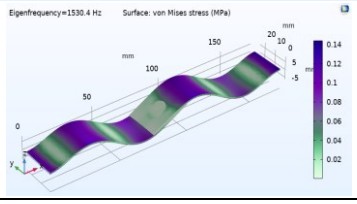	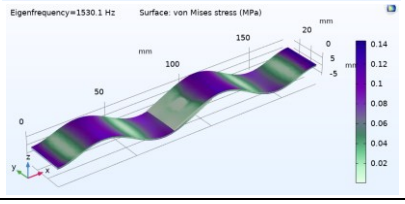	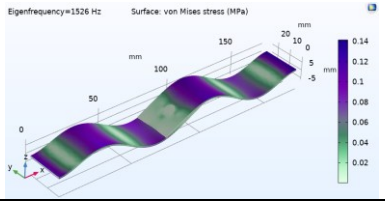

5.5. Vibration test

An eigenfrequency analysis was conducted to investigate the free-vibration behaviour of resistance spot welding (RSW) dissimilar-metal joints formed between low-carbon steel (AISI 1005) and austenitic stainless steel (AISI 304L). Two supports, a cantilever and a fixed-fixed, were used in a modal analysis to determine the effects on their vibration responses.

Intermediary frequency values were obtained in samples dissimilar metal weld AISI 1005 and AISI 304L (1C, 6C, OC) compared to the similar ones, as shown in Figs. 9 and 10. The frequencies showed less stability and greater dispersion in the cantilever support, possibly due to the diversity of elastic modulus and thermal expansion coefficient at the weld contact [73]. The fixed-fixed boundary condition resulted in consistently higher and more uniform eigenfrequencies. However, a few anomalies were observed, suggesting the presence of residual stresses or differences in microstructure resulting from the RSW process.

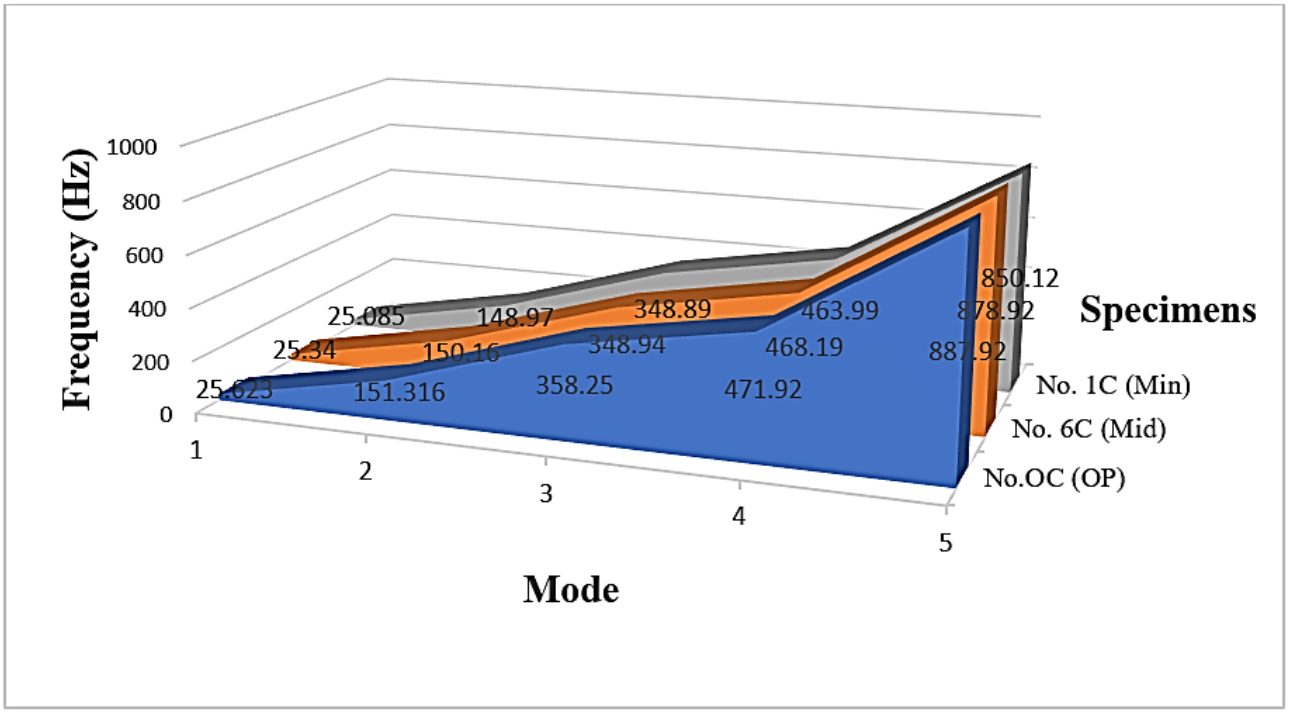

Fig. 9. First degree of freedom-free vibration with cantilever beam (Eigenfrequency (Hz)) of dissimilar AISI 1005 and AISI 304L

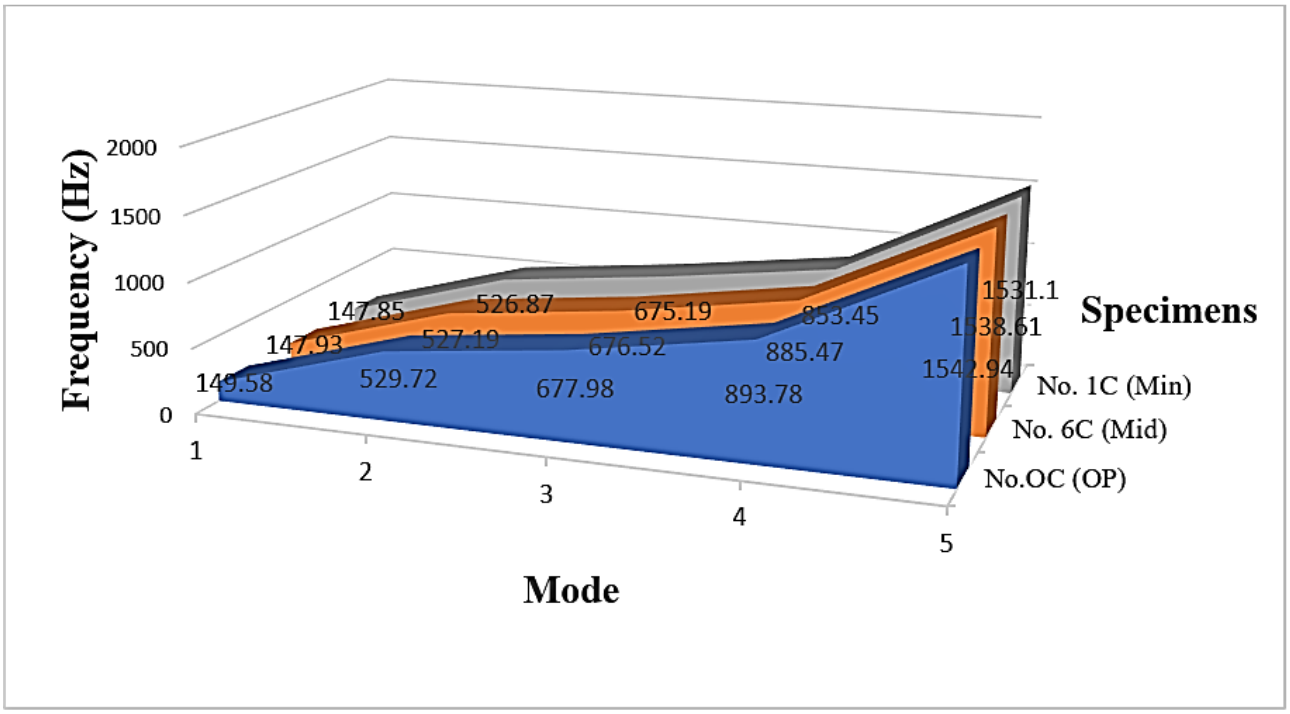

Fig. 10. First degree of freedom-free vibration with fixed-fixed support (Eigenfrequency (Hz)) of dissimilar AISI 1005 and AISI 304L

The summary of Table 8 proves that material qualities and boundary conditions (support) significantly affect vibrational behavior. Dissimilar RSW joints revealed increased susceptibility to local stiffness and the weld metal contact [74, 75].

Table 8. Welding parameters optimum

Material Type	Boundary Condition	Observe
AISI 1005–304L	Cantilever	Intermediate frequencies, high variation
AISI 1005–304L	Fixed-fixed	Improved consistency, moderate frequencies

5.6. Vibration test validation

Tables 9 and 10 show the validation results for the free vibration simulation of RSW joints, comparing simulated eigenfrequencies and experimental measurements. The validation process shows a significant degree of accuracy in general; error percentages remain within suitable engineering limits, verifying the dependability of the simulation technique. With most values within ±3%, the error percentages for dissimilar AISI 1005 and AISI 304L joints (Tables 9 and 10) were relatively low. Under cantilever support, the first two modes showed the most variance; sample 1C came to about −2.9%. In cases with involved material interfaces, this remarkable agreement between simulation and experiment for dissimilar RSW joints improves the numerical modeling even further [76].

Regarding material properties, weld geometry, and boundary conditions, the relatively low error tolerances always support the predictions developed during simulation. A useful instrument for future design optimization and dynamic analysis of RSW structures, the simulation structure also successfully estimated the essential vibrational characteristics of welded joints [77].

Table 9. First degree of freedom-free vibration with cantilever (Eigenfrequency (Hz)) of dissimilar AISI 1005 and AISI 304L validation

Mode	Error (%) OC	Error (%) 6C	Error (%) 1C
1	-0.863	-2.139	-2.993
2	-0.620	-1.599	-2.487
3	1.894	-0.371	0.542
4	2.994	2.178	1.465
5	2.057	1.232	-0.317

Table 10. First degree of freedom-free vibration with fixed-fixed support (Eigenfrequency (Hz)) of dissimilar AISI 1005 and AISI 304L validation

Mode	Error (%) OC	Error (%) 6C	Error (%) 1C
1	1.582	-0.202	0.476
2	-0.346	-0.697	-0.418
3	1.180	0.790	0.761
4	1.940	0.992	-0.662
5	0.819	0.556	0.334

6. Conclusion

The current study investigated the RSW joints of AISI 1005 and AISI 304L under various welding parameters. It examined the simulation of RSW joints of dissimilar metals, the tensile test of RSW joints, and the modeling of vibration tests by COMSOL Multiphysics. The results showed differences in a welding model executed in a joint between dissimilar metals. The possibility of fracture under tensile loads was decreased in the sample OP. According to the tensile-shear test validation, the sample's simulation and experimental values (OP, No.6, and No.1) appeared to have an error percentage of 4.3%, 4.56%, and 4.8%, respectively. The vibration model fixed-fixed support for all samples significantly increased eigenfrequencies and enhanced overall stiffness. Because of its free-end flexibility, the vibration model cantilever supported the structure with lower eigenfrequencies, which allows for more significant deformation under vibrational loads. The sample OP continuously displayed significant eigenfrequencies through both support types, especially in higher modes. This demonstrated the importance of optimum welding parameters in enhancing the dynamic efficiency of welded joints.

Acknowledgment

The authors sincerely thank the National Engineering School of Monastir (ENIM), University of Monastir, LGM, Monastir, Tunisia, and the Polytechnic College of Engineering – Baghdad, Middle Technical University, Baghdad, Iraq, for their valuable technical support, laboratory facilities, and scientific assistance, all of which contributed greatly to the success of this research.

References

[1] N. M. Abbas, S. M. Hassoni, and M. I. Ismail, “Investigate the effect of resistance spot welding pulsation on dissimilar Al–Ti joint on corrosion behavior and mechanical properties,” Advances in Science and Technology Research Journal, vol. 19, no. 11, pp. 466–473, 2025, doi: 10.12913/22998624/209666.

[2] A. K. Hussein, O. S. Barrak, M. M. Hamzah, and S. K. Hussein, “Friction stir welding AA6061-T6 with multi-objective optimization of parameters,” Adv. Sci. Technol. Res. J., vol. 19, no. 10, pp. 162–172, 2025, doi: 10.12913/22998624/207049.

[3] N. A. Husain and H. Ouyang, “Detection of damage in welded structure using experimental modal data,” in J. Phys.: Conf. Ser., vol. 305, no. 1, p. 012120, 2011, doi: 10.1088/1742-6596/305/1/012120.

[4] M. M. Hamzah, O. S. Barrak, I. T. Abdullah, and S. K. Hussein, “Process parameters influence the mechanical properties and nugget diameter of AISI 316 stainless steel during resistance spot welding,” Int. J. Appl. Mech. Eng., vol. 29, no. 2, pp. 79–89, 2024, doi: 10.59441/ijame/186956.

[5] S. S. Edan and R. M. Taha, “Characterization of laser structuring on AISI 304 stainless steel,” NJES, vol. 28, no. 1, pp. 61–66, Apr. 2025, doi: 10.29194/NJES.28010061.

[6] I. M. Husain, O. F. Taresh, G. R. M. Ali, O. S. Barrak, S. K. Hussain, and A. K. Kareem, “Effect of pulses on spot resistance welding of AA1050 aluminum alloy,” in AIP Conf. Proc., vol. 3105, no. 1, Aug. 2024, doi: 10.1063/5.0212205.

[7] H. G. Mohammed, T. L. Ginta, and M. Mustapha, “The investigation of microstructure and mechanical properties of resistance spot welded AISI 316L austenitic stainless steel,” Mater. Today Proc., vol. 46, pp. 1640–1644, 2021, doi: 10.1016/j.matpr.2020.07.258.

[8] C. Wu, Z. Guo, G. Liu, Y. Li, and L. Chen, “Effects of groove shape on microstructure and properties of resistance spot welding joints in WC–10Co/B318 steel,” Int. J. Refract. Met. Hard Mater., vol. 101, p. 105693, 2021, doi: 10.1016/j.ijrmhm.2021.105693.

[9] M. H. Sar, M. H. Ridha, I. M. Husain, O. S. Barrak, and S. K. Hussein, “Influence of welding parameters of resistance spot welding on joining aluminum with copper,” Int. J. Appl. Mech. Eng., vol. 27, no. 2, pp. 217–225, 2022, doi: 10.2478/ijame-2022-0029.

[10] B. Wang et al., “Microstructure and shearing strength of stainless steel/low carbon steel joints produced by resistance spot welding,” J. Mater. Res. Technol., vol. 20, pp. 2668–2679, 2022, doi: 10.1016/j.jmrt.2022.08.041.

[11] S. Rahimi and M. Movahedi, “Resistance spot welding of aluminum to aluminum clad steel sheet: Experimental and theoretical analysis,” J. Manuf. Process., vol. 58, pp. 429–435, 2020, doi: 10.1016/j.jmapro.2020.08.026.

[12] O. S. Barrak, S. Chatti, and S. Ben-Elechi, “Influence of welding parameters on mechanical properties and microstructure of similar low-carbon steel AISI 1005 welding by resistance spot welding,” J. Techniques, vol. 6, no. 1, pp. 45–51, 2024, doi: 10.51173/jt.v6i1.2114.

[13] S. Ren et al., “Post-weld cold working for fatigue strength improvement of resistance spot welded joint of advanced high-strength steel,” J. Mater. Process. Technol., vol. 299, p. 117364, 2022, doi: 10.1016/j.jmatprotec.2021.117364.

[14] A. Arumugam and A. Pramanik, “A review on the recent trends in forming composite joints using spot welding variants,” J. Compos. Sci., vol. 8, no. 4, p. 155, 2024, doi: 10.3390/jcs8040155.

[15] O. S. Barrak, S. Ben-Elechi, and S. Chatti, “Parameters influence on mechanical properties of resistance spot welding: AISI304L/AISI1005,” Pollack Periodica, early access, 2024, doi: 10.1556/606.2024.01142.

[16] G. Chen et al., “Microstructure and mechanical property of WC-10Co/RM80 steel dissimilar resistance spot welding joint,” Mater. Sci. Eng. A, vol. 776, p. 139008, 2020, doi: 10.1016/j.msea.2020.139008.

[17] S. Rached, A. Chaabene, and S. Chatti, “Enhancing friction stir welding performance: Finite element simulation study using filler material,” Ann. Dunarea de Jos Univ. Galati, Fasc. XII, vol. 35, pp. 79–92, 2024.

[18] A. Ghatei-Kalashami et al., “Failure behavior of resistance spot welded advanced high-strength steel: The role of surface condition and initial microstructure,” J. Mater. Process. Technol., vol. 299, p. 117370, 2022, doi: 10.1016/j.jmatprotec.2021.117370.

[19] K. Mahmud et al., “Geometrical degradation of electrode and liquid metal embrittlement cracking in resistance spot welding,” J. Manuf. Process., vol. 61, pp. 334–348, 2021, doi: 10.1016/j.jmapro.2020.11.025.

[20] M. H. Sar et al., “Study the effect of filer material on microstructure of welding the carbon steel in shielded metal arc welding,” J. Mech. Eng. Res. Dev., vol. 43, no. 3, pp. 408–416, 2020.

[21] Y. Ma et al., “Fracture modeling of resistance spot welded ultra-high-strength steel considering the effect of liquid metal embrittlement crack,” Mater. Des., vol. 210, p. 110075, 2021, doi: 10.1016/j.matdes.2021.110075.

[22] L. Mthembu et al., “Model selection in finite element model updating using the Bayesian evidence statistic,” Mech. Syst. Signal Process., vol. 25, no. 7, pp. 2399–2412, 2011, doi: 10.1016/j.ymssp.2011.04.001.

[23] M. S. Fakhri, A. Al-Mukhtar, and I. A. Mahmood, “Investigating spot weld fatigue failure with experimental and finite element analysis

methods," JJMIE, vol. 81, no. 2, 2024, doi: 10.59038/jjmie/180205.
[24] A. E. Sa'ad-Aldeen and S. A. Sarow, "Analyze thermal installation in buildings for different insulations and thicknesses using CFD," Must J. Mater. Eng. Sustain., vol. 1, no. 1, pp. 36–47, Jul. 2025, doi: 10.31272/mjmes.v1i1.2.
[25] A. S. Adkine and S. K. Biradar, "A review of the effects of resistance spot welding on metallurgical and mechanical characteristics," Welding Int., pp. 1–14, 2024, doi: 10.1080/09507116.2024.2419551.
[26] S. Maggiore et al., "A review of structural adhesive joints in hybrid joining processes," Polymers, vol. 13, no. 22, p. 3961, 2021, doi: 10.3390/polym13223961.
[27] F. Lambiase et al., "A state-of-the-art review on advanced joining processes for metal–composite and metal–polymer hybrid structures," Materials, vol. 14, no. 8, p. 1890, 2021, doi: 10.3390/ma14081890.
[28] M. Ishak et al., "Study of resistance spot welding between AISI 301 stainless steel and AISI 1020 carbon steel dissimilar alloys," J. Mech. Eng. Sci., vol. 6, pp. 793–806, 2014, doi: 10.15282/jmes.7.2014.7.0077.
[29] O. S. Barrak, M. M. Hamzah, and S. K. Hussein, "Friction stir spot welding of pure copper (C11000) with pre-holed threaded aluminum alloys (AA5052)," J. Appl. Sci. Eng., vol. 26, no. 8, pp. 1103–1110, 2022, doi: 10.6180/jase.202308_26(8).0006.
[30] S. D. Meshram et al., "Friction stir welding: An alternative to fusion welding for better stress corrosion cracking resistance of maraging steel," J. Manuf. Process., vol. 25, pp. 94–103, 2017, doi: 10.1016/j.jmapro.2016.11.005.
[31] R. Qiu et al., "Characterization of resistance spot welded joints between aluminum alloy and mild steel with composite electrodes," J. Mater. Res. Technol., vol. 24, pp. 1190–1202, 2023, doi: 10.1016/j.jmrt.2023.03.069.
[32] X. Meng et al., "Effect of hold time on resistance spot weldability of aluminium to steel," Sci. Technol. Weld. Join., vol. 27, no. 7, pp. 522–532, 2022, doi: 10.1080/13621718.2022.2080448.
[33] M. Li et al., "Hybrid resistance–laser spot welding of aluminum to steel dissimilar materials: Microstructure and mechanical properties," Mater. Des., vol. 221, p. 111022, 2022, doi: 10.1016/j.matdes.2022.111022.
[34] S. Aslanlar et al., "Effect of welding current on mechanical properties of galvanized chromided steel sheets in electrical resistance spot welding," Mater. Des., vol. 28, no. 1, pp. 2–7, 2007, doi: 10.1016/j.matdes.2005.06.022.
[35] S. Aslanlar et al., "Welding time effect on mechanical properties of automotive sheets in electrical resistance spot welding," Mater. Des., vol. 29, no. 7, pp. 1427–1431, 2008, doi: 10.1016/j.matdes.2007.09.004.
[36] D. Kianersi et al., "Resistance spot welding joints of AISI 316L austenitic stainless steel sheets: Phase transformations, mechanical properties and microstructure characterizations," Mater. Des., vol. 61, pp. 251–263, 2014, doi: 10.1016/j.matdes.2014.04.075.
[37] Z. Wu et al., "Experimental investigation on solid state resistance spot welding," in Proc. ASME IMECE, vol. 58356, 2017, doi: 10.1115/IMECE2017-72581.
[38] M. Ayaz et al., "Enhancing the strength of aluminum–stainless steel spot weld using magnetic pulses," J. Mater. Eng. Perform., 2022, doi: 10.1007/s11665-021-06235-9.
[39] Y. Zhang and D. Sun, "Microstructures and mechanical properties of steel/aluminum alloy joints welded by resistance spot welding," J. Mater. Eng. Perform., vol. 26, pp. 2649–2662, 2017, doi: 10.1007/s11665-017-2731-6.
[40] M. S. M. Mansor et al., "Microstructure and mechanical properties of micro-resistance spot welding between stainless steel 316L and Ti–6Al–4V," Int. J. Adv. Manuf. Technol., vol. 96, pp. 2567–2581, 2018, doi: 10.1007/s00170-018-1688-4.
[41] M. S. Fakhri et al., "Experimental and numerical investigation of mechanical properties and stress intensity factor of dissimilar spot weld joints," J. Mater. Eng. Perform., 2024, doi: 10.1007/s11665-024-10181-7.
[42] M. K. Farhan et al., "Analyzing vibration characteristics: A comparative study of laser vs. spindle systems," NJES, vol. 28, no. 1, pp. 44–51, Apr. 2025, doi: 10.29194/NJES.28010044.
[43] D. Zhao et al., "Dynamic resistance signal–based wear monitoring of resistance spot welding electrodes," Int. J. Adv. Manuf. Technol., 2024, doi: 10.1007/s00170-024-13993-y.
[44] A. H. Majeed and Y. H. Abd, "Experimental study of triple pipe heat exchanger with nanofluids," Must J. Mater. Eng. Sustain., vol. 1, no. 1, pp. 27–35, Jul. 2025, doi: 10.31272/mjmes.v1i1.5.
[45] M. L. Saad et al., "Fuzzy logic model analysis of shear force in aluminium/polyethylene lap joined by hot press," in IOP Conf. Ser.: Mater. Sci. Eng., vol. 518, no. 3, p. 032007, 2019, doi: 10.1088/1757-899X/518/3/032007.
[46] A. Berman and E. J. Nagy, "Improvement of a large analytical model using test data," AIAA J., vol. 21, no. 8, pp. 1168–1173, 1983, doi: 10.2514/3.60140.
[47] J. E. Mottershead et al., "The sensitivity method in finite element model updating: A tutorial," Mech. Syst. Signal Process., vol. 25, no. 7, pp. 2275–2296, 2011, doi: 10.1016/j.ymssp.2010.10.012.
[48] N. A. Abu Husain et al., "Application of the perturbation method with parameter weighting matrix assignments for estimating variability in a set of nominally identical welded structures," in Proc. ASME ESDA, pp. 95–104, 2010, doi: 10.1115/ESDA2010-24272.
[49] N. A. Husain et al., "Parameter selection and stochastic model updating using perturbation methods with parameter weighting matrix assignment," Mech. Syst. Signal Process., vol. 32, pp. 135–152, 2012, doi: 10.1016/j.ymssp.2012.04.001.
[50] M. S. M. Sani et al., "Vibration analysis of resistance spot welding joint for dissimilar plate structure," in IOP Conf. Ser.: Mater. Sci. Eng., vol. 238, no. 1, p. 012017, 2017, doi: 10.1088/1757-899X/238/1/012017.
[51] O. S. Barrak, S. Ben-Elechi, and S. Chatti, "Vibration analysis of resistance spot welding joint of similar metals (carbon steel AISI 1005): A review," J. Techniques, vol. 7, no. 1, pp. 94–104, Mar. 2025, doi: 10.51173/jt.v7i1.2667.
[52] A. Lye et al., "Sampling methods for solving Bayesian model updating problems: A tutorial," Mech. Syst. Signal Process., vol. 159, p. 107760, 2021, doi: 10.1016/j.ymssp.2021.107760.
[53] AWS C1.1M/C1.1-2012: Recommended Practices for Resistance Welding, American Welding Society, 2012.
[54] D. J. Ewins, Modal Testing: Theory, Practice and Application. Hoboken, NJ, USA: Wiley, 2009.
[55] ASM Handbook, Vol. 6A: Welding Fundamentals and Processes, ASM Int., 2011.
[56] COMSOL Multiphysics® Reference Manual, COMSOL AB, 2023.
[57] A. Y. C. Nee, Handbook of Manufacturing Engineering and Technology. Singapore: Springer, 2014.
[58] I. Arrayago, E. Real, and L. Gardner, "Description of stress–strain curves for stainless steel alloys," Mater. Des., vol. 87, pp. 540–552, 2015, doi: 10.1016/j.matdes.2015.08.001.
[59] T. L. Schmitz and K. S. Smith, Mechanical Vibrations: Modeling and Measurement. New York, NY, USA: Springer, 2012, doi: 10.1007/978-3-030-52344-2.

[60] Y. V. Kong et al., "A simple spot weld joint finite element model for vibration analysis," in Mater. Sci. Forum, vol. 911, pp. 112–117, 2018, doi: 10.4028/www.scientific.net/MSF.911.112.
[61] L. Meirovitch, Fundamentals of Vibrations. Long Grove, IL, USA: Waveland Press, 2010.
[62] N. C. Lü et al., "Finite element analysis of residual welding stresses and deformation for a 5A06 aluminum alloy plate," Strength Mater., vol. 52, pp. 532–538, 2020, doi: 10.1007/s11223-020-00204-8.
[63] A. K. Maurya et al., "Influence of heat input on weld integrity of weldments of two dissimilar steels," Mater. Manuf. Process., vol. 38, no. 4, pp. 379–400, 2023, doi: 10.1080/10426914.2022.2075889.
[64] A. Eibeck et al., "Research data supporting…," Apollo – Univ. Cambridge Repository, 2024, doi: 10.17863/CAM.82548.
[65] M. Shojaee et al., "Influence of loading orientation on mechanical properties of spot welds," Int. J. Mech. Sci., vol. 224, p. 107327, 2022, doi: 10.1016/j.ijmecsci.2022.107327.
[66] S. Ren et al., "Numerical modeling from process to residual stress induced in resistance spot welding of DP980 steel," Int. J. Adv. Manuf. Technol., vol. 125, pp. 3563–3576, 2023, doi: 10.1007/s00170-023-10845-z.
[67] H. Moshayedi and I. Sattari-Far, "Resistance spot welding and the effects of welding time and current on residual stresses," J. Mater. Process. Technol., vol. 214, no. 11, pp. 2545–2552, 2014, doi: 10.1016/j.jmatprotec.2014.05.008.
[68] M. Elitas, "Effects of welding parameters on tensile properties and fracture modes of resistance spot welded DP1200 steel," Mater. Testing, vol. 63, no. 2, pp. 124–130, 2021, doi: 10.1515/mt-2020-0019.
[69] W. Zhao et al., "3D finite element analysis and optimization of welding residual stress in the girth joints of X80 steel pipeline," J. Manuf. Process., vol. 66, pp. 166–178, 2021, doi: 10.1016/j.jmapro.2021.04.009.
[70] S. Ao et al., "Determination of residual stress in resistance spot-welded joint by a novel X-ray diffraction," Measurement, vol. 161, p. 107892, 2020, doi: 10.1016/j.measurement.2020.107892.
[71] Y. Yang et al., "Effects of resistance spot welding parameters on microstructure and mechanical properties of dissimilar welded joint of quenching and partitioning steels," Mater. Res. Express, vol. 11, no. 9, p. 096522, 2024, doi: 10.1088/2053-1591/ad791e.
[72] Y. Su et al., "Numerical simulation and experimental investigation of resistance spot welding with initial gap under tensile shear load," J. Manuf. Process., vol. 124, pp. 1102–1111, 2024, doi: 10.1016/j.jmapro.2024.07.027.
[73] R. Kumar et al., "Impact of process parameters of resistance spot welding on mechanical properties and micro-hardness of stainless steel 304 weldments," Int. J. Struct. Integr., vol. 12, no. 3, pp. 366–377, 2021, doi: 10.1108/IJSI-03-2020-0031.
[74] C. Y. Teoh et al., "Structural vibration analysis of weld defects," in AIP Conf. Proc., vol. 2959, no. 1, Nov. 2023, doi: 10.1063/5.0179416.
[75] M. R. A. Shawon et al., "Effect of welding current on the structure and properties of resistance spot welded dissimilar metal joints," J. Inst. Eng. (India) Ser. D, vol. 96, pp. 29–36, 2015, doi: 10.1007/s40033-014-0060-6.
[76] M. F. McGuire, Stainless Steels for Design Engineers. Materials Park, OH, USA: ASM Int., 2008.
[77] H. Zhang and J. Senkara, Resistance Welding: Fundamentals and Applications. Boca Raton, FL, USA: CRC Press, 2011.